Possible multigap type-I superconductivity in the layered boride RuB_2

Jaskaran Singh,[1] Anooja Jayaraj,[1] D. Srivastava,[1,2] S. Gayen,[1] A. Thamizhavel,[3] and Yogesh Singh[1]

[1]*Department of Physical Sciences, Indian Institute of Science Education and Research (IISER) Mohali, Knowledge City, Sector 81, Mohali 140306, India*

[2]*Department of Physics, Central University of Rajasthan*

[3]*Department of Condensed Matter Physics and Material Sciences, Tata Institute of Fundamental Research, Mumbai 400005, India*

(Received 17 March 2017; revised manuscript received 2 January 2018; published 9 February 2018)

The structure of the layered transition-metal borides AB_2 (A = Os, Ru) is built up by alternating T and B layers with the B layers forming a puckered honeycomb. Here we report superconducting properties of RuB_2 with a $T_c \approx 1.5$ K using measurements of the magnetic susceptibility versus temperature T, magnetization M versus magnetic field H, resistivity versus T, and heat capacity versus T at various H. We observe a reduced heat capacity anomaly at T_c given by $\Delta C/\gamma T_c \approx 1.1$ suggesting multigap superconductivity. Strong support for this is obtained by the successful fitting of the electronic specific heat data to a two-gap model with gap values $\Delta_1/k_B T_c \approx 1.88$ and $\Delta_2/k_B T_c \approx 1.13$. Additionally, M versus H measurements reveal a behavior consistent with type-I superconductivity. This is confirmed by comparing the experimental critical field ≈122 Oe obtained from extrapolation to $T = 0$ of the H-T phase diagram, with an estimate of the $T = 0$ thermodynamic critical field ≈114 Oe. Additionally, the Ginzburg-Landau parameter was estimated to be $\kappa \approx 0.1$–0.66. These results strongly suggest multigap type-I superconductivity in RuB_2. We also calculate the band structure and obtain the Fermi surface for RuB_2. The Fermi surface consists of one quasi-two-dimensional sheet and two concentric ellipsoidal sheets very similar to OsB_2. An additional small fourth sheet is also found for RuB_2. RuB_2 could thus be an example of a multigap type-I superconductor.

DOI: 10.1103/PhysRevB.97.054506

I. INTRODUCTION

The discovery of multigap superconductivity in MgB_2 [1,2] has led to a revival of interest and activity in the search for similar behavior in other superconductors. There are now several accepted candidate multigap superconductors such as $NbSe_2$ [3], RNi_2B_2C (R = Lu and Y) [4], $Lu_2Fe_3Si_5$ [5,6], Sr_2RuO_4 [7], and more recently FeSe [8,9]. Multigap superconductors are associated with several anomalous superconducting properties, for example, a reduced heat capacity jump at the superconducting critical temperature $\Delta C/\gamma T_c$, a non-BCS temperature dependence of the upper critical field, and a non-BCS penetration depth versus temperature. These anomalous properties are mostly connected with Fermi surface sheets with very different characters. This is exemplified most clearly in the case of MgB_2 [10–13].

Recently OsB_2, which has a layered structure with puckered honeycomb boron planes alternating with osmium planes stacked along the c axis of an orthorhombic cell, has been studied for its superhardness as well as for its superconducting properties. Several anomalous superconducting properties like upward curvature in the $H_c(T)$ curve, reduced heat capacity anomaly at T_c, non-BCS temperature dependence of the penetration depth, small Ginzburg-Landau parameters $\kappa \sim 1$–2, and a first-order superconducting transition in a magnetic field have been observed for OsB_2 [14,15]. These properties were interpreted as signatures of two-gap superconductivity. A fit by a two-gap model to the T dependent penetration depth data gave the values $\Delta_1 \approx 1.25 k_B T_c$ and $\Delta_2 \approx 1.9 k_B T_c$ for the two gaps, respectively [15]. The Fermi surface of OsB_2 consists of a quasi-two-dimensional sheet and two concentric ellipsoidal sheets [16]. The two gaps were argued to open on the two ellipsoidal Fermi surface sheets which are very similar in character and size [15], unlike the two gaps in MgB_2 which open on two Fermi sheets which are very different in character [13].

However, an alternate view has recently been put forward for these anomalous properties of OsB_2 with proposal of extreme type-I superconductivity (very small κ) and a single but highly anisotropic gap [17].

RuB_2 is isostructural to OsB_2 and is also reported to become superconducting below $T_c \approx 1.5$ K [18]. Although its normal state properties have been studied in detail [14], the superconducting properties have not been explored. Given the anomalous superconducting properties of OsB_2, it would be interesting to make a detailed study of the superconducting properties of RuB_2 to look for similar anomalous properties. In this work we report the superconducting properties of polycrystalline samples of RuB_2. We confirm that RuB_2 exhibits bulk superconductivity below a critical temperature $T_c = 1.5$ K. The magnetization versus magnetic field data suggest type-I superconductivity. We estimate an electron-phonon coupling constant $\lambda_{ep} = 0.39$–0.45 suggesting moderate coupling superconductivity in RuB_2. The extrapolated $T = 0$ critical field $H_c(0) \approx 122$ Oe is small and consistent with type-I superconductivity. The normalized heat capacity jump at T_c was estimated to be $\Delta C/\gamma T_c \approx 1.1$, which is much smaller than the value 1.43 expected for a single-gap s-wave BCS superconductor and suggests multigap superconductivity. This is confirmed by obtaining an excellent fit of the electronic specific heat data below T_c to a phenomenological two-gap model. The fit gave

the gap values $\Delta_1/k_BT_c \approx 1.88$ and $\Delta_2/k_BT_c \approx 1.13$ for the two gaps. The jump in the heat capacity at T_c becomes larger in applied magnetic fields again suggesting type-I behavior. These suggestions are confirmed by estimates of the Ginzburg Landau parameter $\kappa = 0.1$–0.6, which is smaller than the value $1/\sqrt{2} \approx 0.707$, the border between type-I and type-II superconductivity. Thus RuB_2 could be a rare example of a multigap type-I superconductor. Additionally, we calculate the band structure and obtain the Fermi surface of RuB_2. The band structure confirms metallic behavior with majority contribution to the density of states (DOS) at the Fermi energy (ϵ_F) coming from Ru $4d$ and B $2p$ orbitals. We calculate the total DOS for both spin directions $\epsilon_F = 1.17$ states/eV f.u., where "f.u." stands for "formula unit." This value is similar to the value reported for OsB_2 [14]. The Fermi surface consists of four sheets. There is one quasi-two-dimensional corrugated tubular sheet and two concentric ellipsoidal sheets, very similar to OsB_2 [14]. An additional small fourth sheet is found which was not obtained for OsB_2.

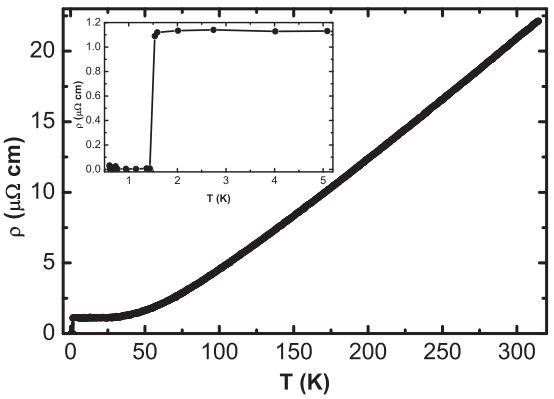

FIG. 1. Electrical resistivity ρ vs temperature T for RuB_2 measured in zero magnetic field between $T = 0.4$ and 310 K. The inset shows the data below $T = 5.5$ K to highlight the abrupt drop at $T_c = 1.5$ K signaling the transition to the superconducting state.

II. EXPERIMENTAL AND THEORETICAL METHODS

Polycrystalline samples of RuB_2 were synthesized by arc-melting stoichiometric ratios of Ru (5N, Alfa Aesar) and B (6N, Alfa Aesar) 5–10 times to promote homogeniety [14]. Powder x-ray diffraction confirmed that the synthesized material is single phase and a refinement of the powder pattern gave lattice parameters which match well with the reported values [14]. The dc magnetic susceptibility χ versus temperature data in the temperature T range $T = 0.280$ K to 2 K and magnetization M versus field H data at $T = 310$ mK were measured using a He3 insert in a SQUID magnetometer from Cryogenics Limited, UK. The heat capacity C data from 85 mK to 3 K was measured using the dilution refrigerator (DR) option of a Quantum Design Physical Property Measurement System (QD-PPMS). The electrical transport from 300 mK to 300 K was measured using the He3 insert in a QD-PPMS. The first-principles density functional theory (DFT) calculations were done using the QUANTUM-ESPRESSO code [19]. Electronic exchange and correlation are described using the generalized gradient approximation (GGA) using Perdew-Bruke-Ernzerhof functional [20]. In the DFT calculation, spin-orbit coupling was not included. However, we have used scalar relativistic potential which takes scalar relativistic effects into account.

III. ELECTRICAL RESISTIVITY

The electrical resistivity ρ versus temperature T data for RuB_2 measured with an excitation current of 5 mA in zero applied magnetic field are shown in Fig. 1 between $T = 0.5$ K and 315 K. The $T = 315$ K value of resistivity is $\rho(315\text{ K}) \approx 22.5\ \mu\Omega$ cm and the residual resistivity is $\rho(1.6\text{ K}) \approx 1.1\ \mu\Omega$ cm giving a residual resistivity ratio (RRR) ≈ 21. The inset in Fig. 1 shows the $\rho(T)$ data below $T = 5.25$ K to highlight the sharp drop to zero resistance below $T_c = 1.5$ K signaling the onset of superconductivity in RuB_2.

IV. MAGNETIC PROPERTIES

Figure 2 shows the results of magnetic measurements on RuB_2. Figure 2(a) shows the temperature dependence of the zero-field-cooled (ZFC) volume magnetic susceptibility χ_v normalized by $1/4\pi$. The data were measured in a field of 10 Oe between 0.28 K and 1.8 K. The sharp drop in χ_v to diamagnetic values below ≈ 1.55 K confirms the onset of the superconducting state. The inset in Fig. 2(a) shows the $d\chi_v/dT$ vs T data and the peak position is taken as the superconducting critical temperature $T_c = 1.5$ K. The full width at half maximum (FWHM) of the peak in $d\chi_v/dT$ gives an estimate of the superconducting transition width and is $\approx$50 mK. The χ_v data have not been corrected for the demagnetization factor N. Thus the observed value is $4\pi\chi_v = \frac{-1}{1-N}$ and therefore larger than -1 expected for 100% superconducting volume fraction. Assuming 100% superconducting volume fraction we estimate $N \approx 0.32$ from the data shown in Fig. 2(a). However, often in polycrystalline samples the superconducting fraction is smaller than 100% and to estimate the actual superconducting fraction one needs the value of N. For idealized shapes of samples, N has been calculated. For example, $N = 1/3$ for a sphere and 1 for an ellipsoid of revolution. Our sample is an irregular shaped piece broken from an arc-melted button and looks like a squashed ellipsoid with dimensions $a \approx b = 1.61$ mm $\neq c = 1.35$ mm. We therefore approximate our irregular shaped sample with a prolate ellipsoid with $c/a \approx 0.83$. For such an object, $N \approx 0.38$ [21]. Using this value of N we find a superconducting volume fraction of $\approx 90\%$.

Figure 2(b) shows the volume magnetization M_v normalized by $1/4\pi$ versus magnetic field H for RuB_2 measured at a temperature $T = 310$ mK, well inside the superconducting state. The shape of the $4\pi M_v$ vs H data are very different from those expected for typical type-II superconductors but are similar to that expected for a type-I superconductor with demagnetization factors. To account for demagnetization effects the magnetization can be plotted versus an effective magnetic field $H_{\text{eff}} = H - NM$. This has been done using the $N \approx 0.38$ estimated above and the resulting $M(H_{\text{eff}})$ data are shown in Fig. 2(b), inset. These data look like the behavior expected for a type-I superconductor. The slight negative slope of the data at the transition most likely occurs from a slightly overestimated N.

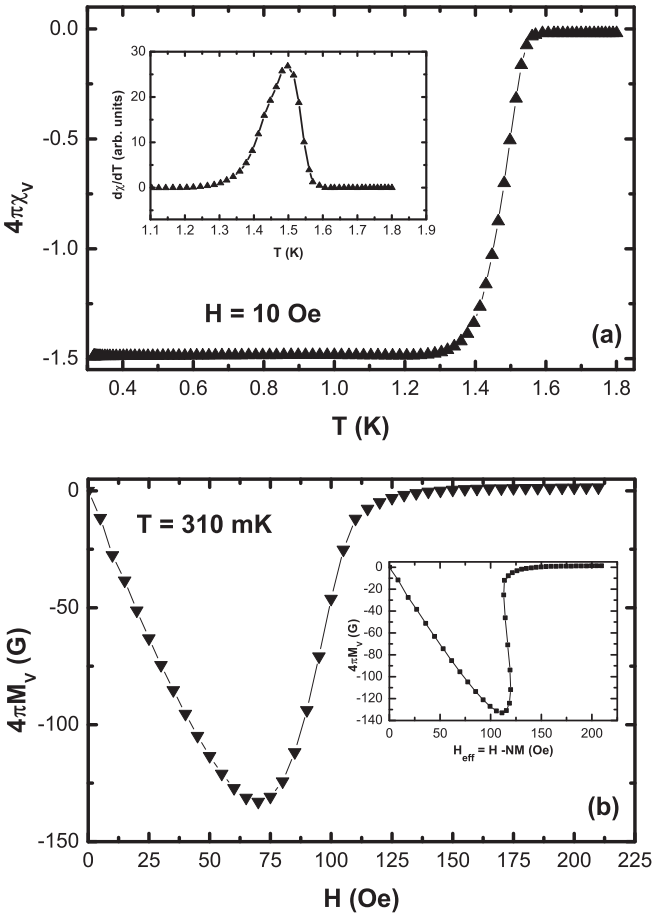

FIG. 2. (a) Temperature T dependence of the zero field cooled (ZFC) dimensionless volume susceptibility χ_v in terms of the superconducting volume fraction $4\pi\chi_v$ of RuB_2 measured in a magnetic field $H = 10$ Oe. At low T, the $4\pi\chi_v$ values are more negative than -1 due to demagnetization effects. The inset shows the $d\chi/dT$ vs T data to highlight the superconducting transition at $T_c = 1.5$ K. (b) The volume magnetization M_v normalized by $1/4\pi$ vs applied magnetic field H measured at $T = 310$ mK. The inset shows the $4\pi M_V$ vs effective magnetic field $H_{\rm eff} = H - NM$ corrected for the demagnetization effects. These data show behavior typical of type-I superconductivity.

V. HEAT CAPACITY

Figure 3(a) shows the specific heat C versus T data for RuB_2 measured between $T = 85$ mK and 3 K in magnetic fields $H = 0$ Oe and $H = 250$ Oe. A sharp anomaly near $T_c = 1.5$ K in the $H = 0$ data confirms bulk superconductivity in RuB_2. The data at $H = 250$ Oe doesn't show any signature of superconductivity and will be used as the normal state data. We will later show that this field is indeed much higher than the estimated critical field. The $C(T)$ data at $H = 250$ Oe were fit by the expression $C = \gamma_n T + \beta T^3$ where γ_n is the normal state Sommerfeld coefficient and the second term is the contribution from the lattice. The fit shown as the solid curve through the $H = 250$ Oe data in Fig. 3(a) gave the values $\gamma_n = 1.65(2)\,\mathrm{mJ/mol\,K^2}$ and $\beta = 0.014(2)\,\mathrm{mJ/mol\,K^4}$.

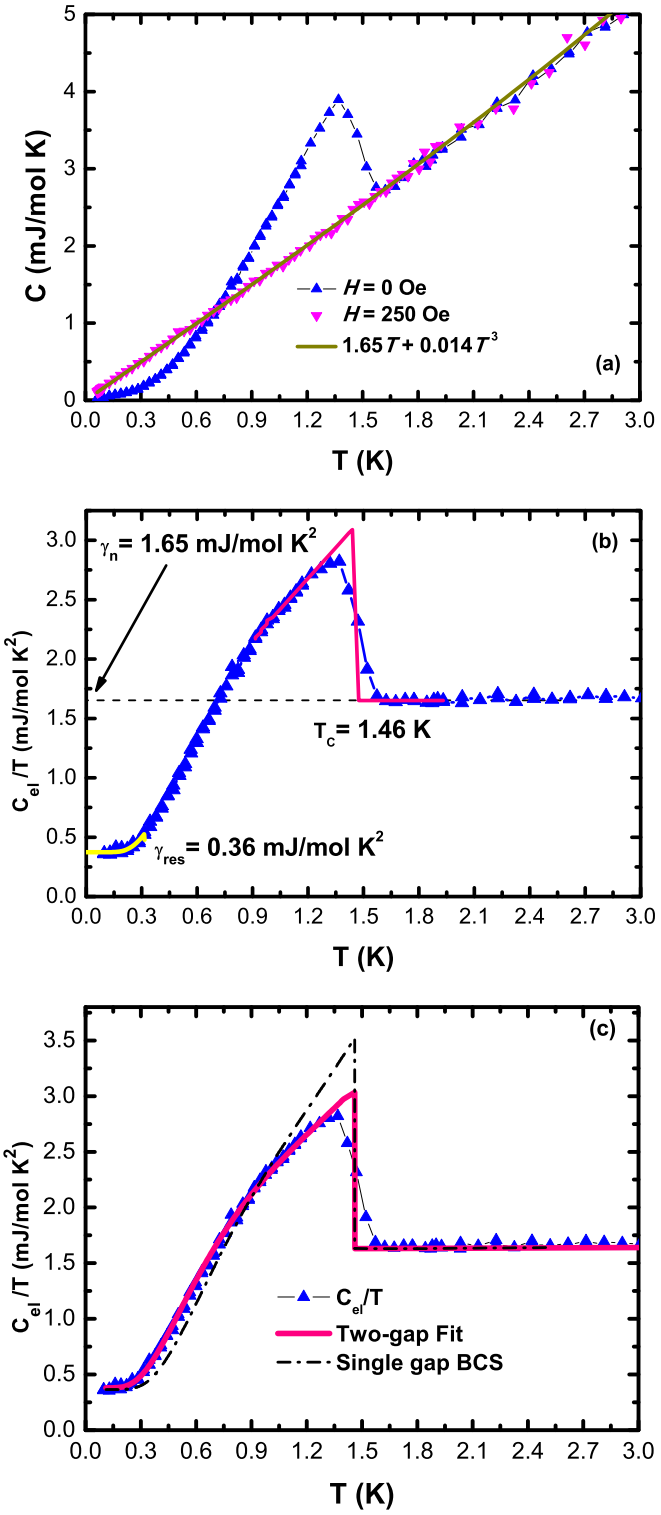

FIG. 3. (a) Specific heat C vs T for RuB_2 measured in magnetic fields $H = 0$ and 250 Oe. The solid curve through the 250 Oe data is a fit by the expression $C = \gamma T + \beta T^3$. (b) The electronic specific heat divided by temperature C_{el}/T vs T for RuB_2. An equal entropy construction is shown to give a $T_c = 1.46$ K and $\Delta C/\gamma T_c = 1.1$, where $\gamma = \gamma_n - \gamma_{\rm res}$. (c) A two-gap model fit (solid curve) to the C_{el} data and expectation for a single BCS gap (dash-dot curve) (see text for details).

This value of β gives a Debye temperature of $\theta_D = 720(30)$ K which is similar to the value found previously [15]. The lattice contribution βT^3 to the total specific heat $C(T)$ can be subtracted to get the electronic contribution $C_{el}(T)$. The $C_{el}(T)$ so obtained is shown in Fig. 3(b). The sharp anomaly at T_c as well as the exponential fall at the lowest temperatures expected for s-wave superconductors is clearly visible. We also note that C_{el} tends to a finite value as $T \to 0$ suggesting some nonsuperconducting fraction in the sample. The data below ≈ 0.3 K were fit by the expression $C_{el}/T = \gamma_{\rm res} + (A/T)\exp(-\Delta/T)$, where $\gamma_{\rm res}$ is the residual Sommerfeld coefficient from the nonsuperconducting fraction of the sample and the second term is a phenomenological exponential decay expected for a gapped system. The fit shown as the solid curve through the data below $T \approx 0.3$ K in Fig. 3(b) gives the value $\gamma_{\rm res} = 0.36$ mJ/mol K^2. With the total $\gamma_n = 1.65$ mJ/mol K^2 and the residual nonsuperconducting $\gamma_{\rm res} = 0.36$ mJ/mol K^2, the superconducting contribution becomes $\gamma_s = 1.29$ mJ/mol K^2. This suggests that ≈22% of the sample volume is nonsuperconducting.

We can now analyze the specific heat jump height at T_c. The jump ΔC at T_c is normalized as $\Delta C/\gamma T_c$, where γ is the Sommerfeld coefficient of the superconducting part. The superconducting transition can be broadened and the jump height suppressed in real materials due to a distribution of T_c arising from sample inhomogeneities or disorder. To get a better estimate of ΔC and T_c we use an entropy-conserving construction. In such a construction the C_{el} data just below the maximum of the anomaly is fit by a polynomial and extrapolated to higher temperatures. The entropy is then evaluated and equated to the normal state entropy $\gamma_n T_c$. Such a construction gave the jump height $\Delta C/T_c = 3.07 - 1.65 = 1.42$ mJ/mol K^2 and $T_c = 1.46$ K as shown in Fig. 3(b). The T_c found by this entropy-conserving construction is quite close to the onset temperature 1.5 K indicating the sharp transition and suggesting a very good sample quality with very little disorder and inhomogeneities. Using the above $\Delta C/T_c = 1.42$ mJ/mol K^2 and the superconducting contribution $\gamma_s = 1.29$ mJ/mol K^2 we estimate $\Delta C/\gamma_s T_c = 1.44/1.29 \approx 1.12$. This value is much smaller than the value 1.43 expected for a single-gap s-wave superconductor. The reduced value of $\Delta C/\gamma T_c$ is similar to observations for MgB_2 [10] and OsB_2 [14,15] and suggests multigap superconductivity.

To confirm this possibility we have attempted to fit our $C_{el}(T)$ data below T_c to a phenomenological two-gap model as has been reported for example for MgB_2 [22]. The $T = 0$ value of the two superconducting gaps Δ_1 and Δ_2, the critical temperature T_c, and the fractional contribution of the first band x were the three fit parameters. An excellent fit, shown in Fig. 3(c) as the solid curve through the C_{el}/T data below T_c, was obtained with the fit parameters $\Delta_1/k_B T_c \approx 1.88$, $\Delta_2/k_B T_c \approx 1.13$, $T_c \approx 1.47$ K, and $x = 0.58$. If we compare the values of the two gaps we estimate above to the single band BCS value $\Delta/k_B T_c = 1.76$ we see that our values agree with the theorem that for a two-gap superconductor one of the gaps will always be larger than the BCS value while the second gap will always be smaller [23]. For comparison, we also show in Fig. 3(c) the simulated data for a superconductor with a single BCS gap with $T_c = 1.47$ K which clearly doesn't match the data. Thus the heat capacity data in Fig. 3 strongly indicate that RuB_2 could be a two-gap superconductor.

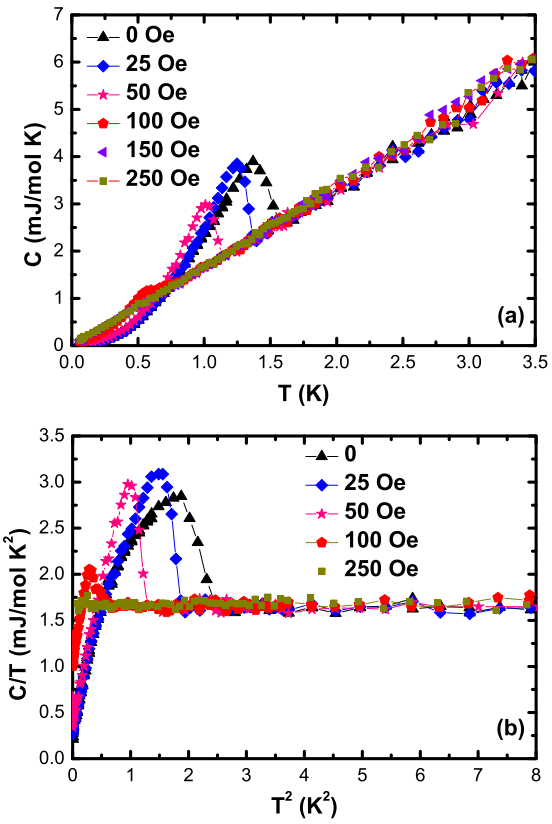

FIG. 4. (a) Specific heat C vs T for RuB_2 measured in various magnetic fields H. (b) C divided by temperature C/T vs T^2 for RuB_2 at various H.

Figure 4(a) shows the specific heat C versus T data for RuB_2 measured between $T = 85$ mK and 3.5 K at various applied magnetic fields H. All data were measured by cooling in zero field to the lowest temperature and then measuring while warming up in the desired magnetic field. As expected, the SC transition is pushed to lower temperatures in increasing fields and is not observed down to the lowest temperature for fields $H \geqslant 150$ Oe. The specific heat divided by temperature C/T versus T at various magnetic fields is plotted in Fig. 4(b). From Fig. 4(b) we observe that the magnitude of the peak at T_c initially increases in a magnetic field. In a magnetic field the transition for a type-I superconductor becomes first order. Thus one should in principle observe a diverging anomaly at T_c. In real materials, however, the anomaly is broadened due to sample inhomogeneity and as a consequence the anomaly looks like a jump larger than that in zero field. Thus the observed behavior in Fig. 4(b) also points to type-I superconductivity in RuB_2. This is similar to what was observed for OsB_2 [15] and for other type-I superconductors like $ScGa_3$ and $LaGa_3$ [24,25] and $YbSb_2$ [26]. This is consistent with the magnetization data of Fig. 2(b), inset, which also suggest type-I superconductivity.

The above value of γ can be used to estimate the density of states at the Fermi energy (ϵ_F) for both spin directions $N(\epsilon_F)$ by using the expression $\gamma = \frac{\pi^2}{6} k_B^2 N(\epsilon_F)$. Using $\gamma = 1.65$ mJ/mol K^2 we obtain $N(\epsilon_F) \approx 1.40$ states/eV f.u. We

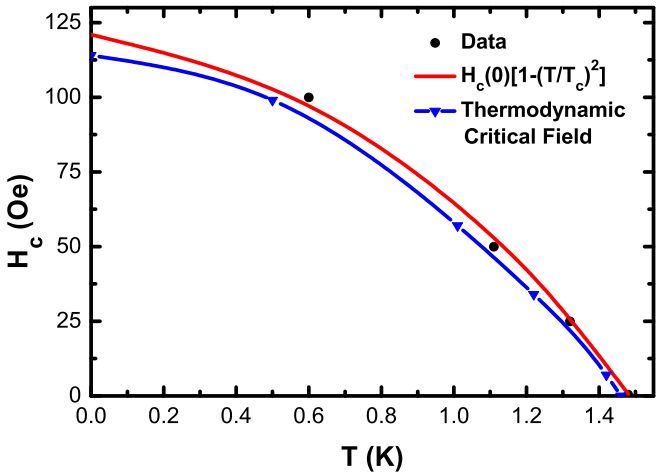

FIG. 5. Critical field H_C vs T data extracted from the heat capacity C vs temperature T at various H. The solid curve through the data is a fit to the phenomenological BCS expression. The thermodynamic critical field $H_{tc}(T)$ obtained from the $C(T)$ data is also plotted for comparison. The solid curve through the $H_{tc}(T)$ data is a guide to the eye (see text for details).

will compare this value with estimations from band structure calculations later.

VI. SUPERCONDUCTING PARAMETERS

The $C(T,H)$ data presented above were used to extract the critical temperature at various magnetic fields. The critical field H_c versus T data thus obtained is shown in Fig. 5. The data were fit by the phenomenological expression $H_c(T) = H_c(0)[1 - (\frac{T}{T_c})^2]$ with $H_c(0)$ and T_c as fitting parameters, where $H_c(0)$ is the zero temperature critical field. The fit, shown as the solid curve through the data in Fig. 5, extrapolated to $T = 0$ gave the values $H_c(0) = 122$ Oe and $T_c = 1.48$ K. The satisfactory fit to the above expression suggests BCS superconductivity in RuB_2.

An estimate for the T dependent thermodynamic critical field $H_{tc}(T)$ can be made from the electronic heat capacity data $C_{el}(T)$ using the expression $[\mu_0 H_{tc}(T)]^2/2 = F_{en} - F_{es} = -\gamma(T^2 + T_c^2)/2 + \int_T^{T_c} C_{el}(T)dT + T\int_0^T \frac{C_{el}(T)}{T}dT$, where F_{en} and F_{es} are the electronic free energy in the normal and superconducting state, respectively [27]. In particular, the $T = 0$ thermodynamic critical field $H_{tc}(0)$ can be estimated by inserting $T = 0$ in the above expression giving $(\mu_0 H_{tc}(0))^2/2 = -\gamma T_c^2/2 + \int_0^{T_c} C_{el}(T)dT$. Using $\gamma_s = 1.3$ mJ mol K^2 and $T_c = 1.46$ K obtained from an equal entropy construction above, we estimate the $T = 0$ thermodynamic critical field $H_{tc}(0) \approx 114$ Oe. This is slightly smaller but close to the estimate 122 Oe made from the H-T phase diagram and suggests type-I superconductivity in RuB_2. This is supported by estimates of the Ginzburg Landau parameter below. For comparison with the experimental H-T diagram obtained from $C(T,H)$ data, the $H_{tc}(T)$ estimated by using the above expression are also shown in Fig. 5.

The electron-phonon coupling λ_{ep} can be estimated using McMillan's formula [28], which relates the superconducting transition temperature T_c to λ_{ep}, the Debye temperature θ_D, and the Coulumb pseudopotential μ^*. This formula can be inverted to get λ_{ep} in terms of the other parameters,

$$\lambda_{ep} = \frac{1.04 + \mu^* \ln\left(\frac{\theta_D}{1.45T_c}\right)}{(1 - 0.62\mu^*)\ln\left(\frac{\theta_D}{1.45T_c}\right) - 1.04}.$$

Using, $\theta_D = 700$ K obtained from heat capacity measurements above and using $T_c = 1.5$ K, we get $\lambda_{ep} = 0.37$ and 0.45 for $\mu^* = 0.1$ and 0.15, respectively. These values are slightly smaller than values obtained for OsB_2 [14] consistent with a slightly smaller T_c compared to OsB_2. These values of λ_{ep} are consistent with previous theortical values [29] and suggest moderate-coupling superconductivity in RuB_2. The corresponding value for MgB_2 is $\lambda_{ep} \approx 1$ [30].

We now estimate the $T = 0$ values of the penetration depth $\lambda(0)$ and coherence length $\xi(0)$. RuB_2 has two formulas units per unit cell. This means that there are four electrons in one unit cell volume $V = 53.84$ Å^3. Therefore, the electron density is $n = 4/V = 7.4 \times 10^{-2}$ Å^{-3}. Assuming a spherical Fermi surface, we can use the above value of n to estimate the Fermi wave vector $k_F = (3n\pi^2)^{1/3} = 1.3$ Å^{-1}. The London penetration depth is given by $\lambda(0) = (m^*/\mu_0 n e^2)^{1/2}$, where we take the effective mass m^* as the free electron mass m_e. Putting in values gives us $\lambda(0) \approx 47$ nm. The BCS coherence length can be estimated using the expression $\xi = \frac{0.18\hbar^2 k_F}{k_B T_c m^*}$ ≈ 0.45 μm. The Ginzburg Landau (GL) parameter can now be estimated as $\kappa = 0.96\lambda(0)/\xi \approx 0.1$ which is much smaller than the value $1/\sqrt{2} \approx 0.707$ separating type-I and type-II superconductivity. The above value of κ suggests that RuB_2 is an extreme type-I superconductor. This is consistent with the low H_c and the $M(H_{\rm eff})$ data presented above. The mean free path l can be estimated using the expression $l = v_F\tau$, where the Fermi velocity is $v_F = \hbar k_F/m^*$ and the scattering time is given by the expression for the Drude conductivity $\tau = m^*/ne^2\rho$. Using $m^* = m_e$ and the residual resistivity value $\rho(1.6\ {\rm K}) = 1.1\ \mu\Omega\,{\rm cm}$, we estimate $l \approx 72$ nm. From the above estimates of ξ and l we conclude that $\xi \gg l$, making RuB_2 a dirty limit superconductor. For a dirty limit superconductor we can make another estimate of the GL parameter as $\kappa = 0.75\lambda(0)/l \approx 0.66 < 0.707$, again consistent with type-I behavior. We add that the estimation of the mean free path l is often affected by grain boundary scatterings, which can cause an underestimation of l. Thus the evaluated $\kappa \approx 0.66$ is an upper limit making our inference of type-I superconductivity even stronger.

VII. BAND STRUCTURE AND FERMI SURFACE

RuB_2 crystallizes in the orthorhombic crystal system, space group $Pmmn$ (no. 59). Each unit cell contains two formula units (two Ru atoms and four B atoms). The ionic and lattice relaxation were performed to optimize the crystal structure by using variable cell relaxation. We have used an energy cutoff of 55 Ry for the plane wave basis. The Brillouin zone integration is conducted with a $11 \times 18 \times 13$ Monkhorst-pack grid for the K-point sampling. In the optimized crystal structure, the forces on all the atoms are less than 10^{-4} Ry/au. The calculated lattice parameters of the optimized RuB_2 compound along

TABLE I. Lattice parameters obtained from relaxing the experimental unit cell of RuB_2.

Lattice parameters (Å)	Experimental	Calculated	% Error
a	4.644795	4.66487	0.43
b	2.865153	2.89674	1.1
c	4.045606	4.05224	0.16

with the experimental values are tabulated in Table I. The calculated lattice parameters are within 1% of the experimental values [14].

The electronic band structure of RuB_2 is shown in Fig. 6. It can be seen that several energy bands are crossing the Fermi level E_F confirming that RuB_2 is a metal. Figure 7 shows the total and partial density of states (DOS) in units of states/eV showing the contribution of individual elements and orbitals to the DOS at various energies measured from the Fermi energy E_F. From Fig. 7 it can be seen that the $5d$ orbital of Ru and the $2p$ orbital of B make the main contributions to the density of states in the vicinity of the Fermi level. The total DOS at ϵ_F is found to be $N(\epsilon_F) = 1.15$ states/eV f.u. for both spin directions. This value is slightly smaller than the value $N(\epsilon_F) = 1.40$ states/eV f.u. estimated from the experimental value of γ. An estimate for the electron-phonon coupling constant λ_{ep} can be made using the following relation: $N(\epsilon_F)$ from heat capacity = [$N(\epsilon_F)$ from band structure] $(1 + \lambda_{ep})$.

A comparison of the above experimental and theoretical values of $N(\epsilon_F)$ gives $\lambda_{ep} \approx 0.22$ which is close to but slightly smaller than the values obtained above using McMillan's formula.

We have also obtained the Fermi surface for RuB_2. The merged Fermi surface within the first Brillouin zone is shown in Fig. 8. The Fermi surface consists of four FS sheets: one quasi-two-dimensional tubular sheet and two concentric ellipsoidal sheets very similar to OsB_2 [16]. An additional small fourth sheet nested inside the tubular sheet is also found for RuB_2.

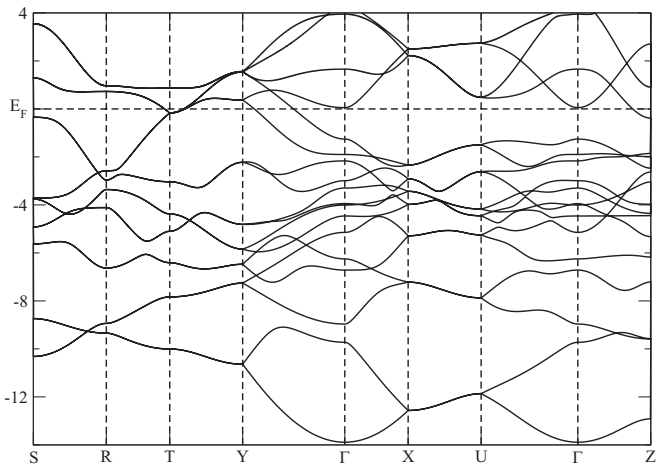

FIG. 6. Calculated electronic band structure of orthorhombic RuB_2 along high symmetric points. E_F represents the Fermi level, which is set at 0 eV.

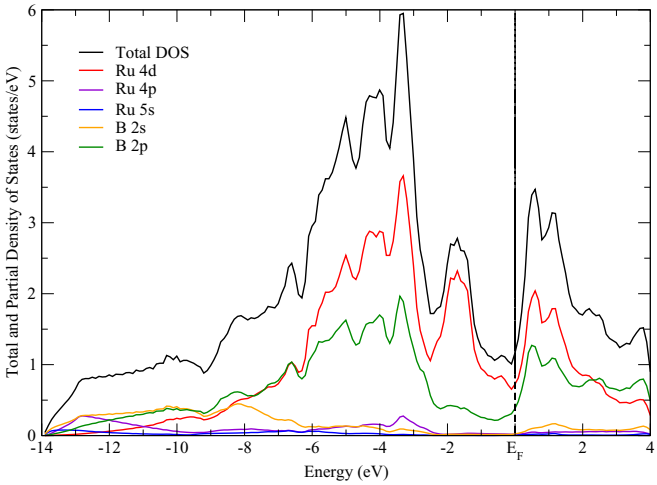

FIG. 7. Calculated total density of states (DOS) and partial density of states (PDOS) for RuB_2. E_F represents the Fermi energy and is set at 0 eV.

VIII. SUMMARY AND DISCUSSION

Using electrical resistivity $\rho(T)$, magnetic susceptibility $\chi(T)$, magnetization $M(H)$, and specific heat $C(T,H)$ data we have confirmed bulk superconductivity in RuB_2 with a superconducting critical temperature $T_c = 1.5$ K. The $T = 0$ critical field is estimated to be $H_c(0) = 122$ Oe. The magnitude of the anomaly in specific heat at T_c in zero field is observed to be $\Delta C/\gamma_s T_c \approx 1.1$, which is much smaller than the value 1.43 expected for a single-gap BCS superconductor. This observation is similar to what has previously been observed for MgB_2 and OsB_2, and suggests multigap superconductivity in RuB_2. This is confirmed by the excellent fitting of the electronic specific heat below T_c to a two-gap model with the value of the two gaps estimated as $\Delta_1/k_B T_c \approx 1.88$ and $\Delta_2/k_B T_c \approx 1.13$. The value of $\Delta C/\gamma T_c$ in a magnetic field becomes larger than its zero field value strongly indicating type-I behavior. This is also similar to what was observed earlier for OsB_2 and also for other candidate type-I superconductors like $ScGa_3$ and $LaGa_3$ [24] and $YbSb_2$ [26]. The $M(H_{\rm eff})$ behavior are also consistent with type-I superconductivity. This is confirmed by

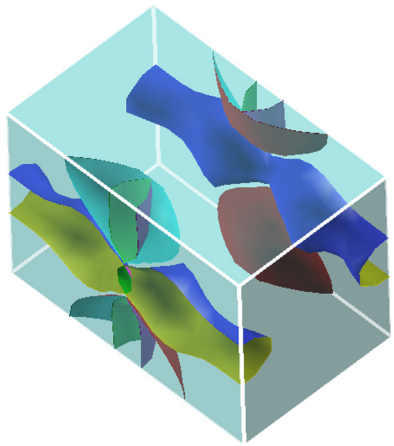

FIG. 8. Merged Fermi surface (FS) for RuB_2 consisting of four different sheets. The parallelepiped is in the first Brillouin zone.

estimates of the Ginzburg-Landau parameter κ which comes out to be $\kappa \approx 0.1$–$0.6 < 0.707$. These results strongly suggest that RuB_2 is a rare alloy type-I superconductor and may be the first multigap type-I superconductor. We note that both $YbSb_2$ ($\kappa \approx 0.05$ and $\Delta C/\gamma T_c <$ BCS) [26] and boron-doped SiC ($\kappa \approx 0.35$ and $\Delta C/\gamma T_c <$ BCS) [31] have been reported as type-I superconductors and have specific heat anomalies smaller than expected for single band BCS superconductivity. However, both reported materials were multiphase samples and, in $YbSb_2$, an additional superconducting phase with a lower T_c than the bulk T_c was also observed, making it complicated to estimate intrinsic superconducting parameters. Thus RuB_2 seems to be the best candidate for two-gap type-I superconductivity so far.

However, a scenario (anisotropic type-I superconductivity) like the one recently suggested for OsB_2 [17] could also be at play in RuB_2 and future work like imaging of magnetic flux entering the material may be useful to confirm the type of superconductivity in RuB_2.

ACKNOWLEDGMENTS

We thank the X-ray facility at IISER Mohali. J.S. acknowledges UGC-CSIR India for a fellowship. D.S. thanks DST, India for INSPIRE faculty award (No. DST/INSPIRE/04/2015/000579). Y.S. acknowledges DST, India for support through Ramanujan Grant No. SR/S2/RJN-76/2010 and through DST Grant No. SB/S2/CMP-001/2013.

[1] F. Bouquet, R. A. Fisher, N. E. Phillips, D. G. Hinks, and J. D. Jorgensen, Phys. Rev. Lett. **87**, 047001 (2001).
[2] H. J. Choi, D. Roundy, H. Sun, M. L. Cohen, and S. G. Louie, Nature (London) **418**, 758 (2002).
[3] E. Boaknin, M. A. Tanatar, J. Paglione, D. Hawthorn, F. Ronning, R. W. Hill, M. Sutherland, L. Taillefer, J. Sonier, S. M. Hayden, and J. W. Brill, Phys. Rev. Lett. **90**, 117003 (2003).
[4] S. V. Shulga, S.-L. Drechsler, G. Fuchs, K.-H. Müller, K. Winzer, M. Heinecke, and K. Krug, Phys. Rev. Lett. **80**, 1730 (1998).
[5] Y. Nakajima, T. Nakagawa, T. Tamegai, and H. Harima, Phys. Rev. Lett. **100**, 157001 (2008).
[6] R. T. Gordon, M. D. Vannette, C. Martin, Y. Nakajima, T. Tamegai, and R. Prozorov, Phys. Rev. B **78**, 024514 (2008).
[7] Y. Maeno, T. M. Rice, and M. Sigrist, Phys. Today **54**, 42 (2001), and references therein.
[8] J. K. Dong, T. Y. Guan, S. Y. Zhou, X. Qiu, L. Ding, C. Zhang, U. Patel, Z. L. Xiao, and S. Y. Li, Phys. Rev. B **80**, 024518 (2009).
[9] M. L. Amig, V. A. Crivillero, D. G. Franco, and G. Nieva, J. Phys.: Conf. Ser. **568**, 022005 (2014).
[10] S. L. Budko, G. Lapertot, C. Petrovic, C. E. Cunningham, N. Anderson, and P. C. Canfield, Phys. Rev. Lett. **86**, 1877 (2001).
[11] Z. X. Shi, M. Tokunaga, T. Tamegai, Y. Takano, K. Togano, H. Kito, and H. Ihara, Phys. Rev. B **68**, 104513 (2003).
[12] F. Manzano, A. Carrington, N. E. Hussey, S. Lee, A. Yamamoto, and S. Tajima, Phys. Rev. Lett. **88**, 047002 (2002).
[13] E. A. Yelland, J. R. Cooper, A. Carrington, N. E. Hussey, P. J. Meeson, S. Lee, A. Yamamoto, and S. Tajima, Phys. Rev. Lett. **88**, 217002 (2002).
[14] Y. Singh, A. Niazi, M. D. Vannette, R. Prozorov, and D. C. Johnston, Phys. Rev. B **76**, 214510 (2007).
[15] Y. Singh, C. Martin, S. L. Bud'ko, A. Ellern, R. Prozorov, and D. C. Johnston, Phys. Rev. B **82**, 144532 (2010).
[16] M. Hebbache, Phys. Status Solidi RRL **3**, 163 (2009).
[17] J. Bekaert, S. Vercauteren, A. Aperis, L. Komendova, R. Prozorov, B. Partoens, and M. Milosevic, Phys. Rev. B **94**, 144506 (2016).
[18] J. M. Vandenberg, B. T. Matthias, E. Corenzwit, and H. Barz, Mater. Res. Bull. **10**, 889 (1975).
[19] P. Giannozzi *et al.*, J. Phys.: Condens. Matter **21**, 395502 (2009).
[20] J. P. Perdew, K. Burke, and M. Ernzerhof, Phys. Rev. Lett. **77**, 3865 (1996).
[21] C. P. Poole, Jr., H. A. Farach, R. J. Creswick, and R. Prozorov, *Superconductivity* (Elsevier, Amsterdam, 2007).
[22] F. Bouquet, Y. Wang, R. A. Fisher, D. G. Hinks, J. D. Jorgensen, A. Junod, and N. E. Phillips, Eur. Phys. Lett. **56**, 856 (2001).
[23] V. Z. Kresin and S. A. Wolf, Physica C **169**, 476 (1990).
[24] E. Svanidze and E. Morosan, Phys. Rev. B **85**, 174514 (2012).
[25] S. Yonezawa and Y. Maeno, Phys. Rev. B **72**, 180504(R) (2005).
[26] L. L. Zhao, S. Lausberg, H. Kim, M. A. Tanatar, M. Brando, R. Prozorov, and E. Morosan, Phys. Rev. B **85**, 214526 (2012).
[27] M. Tinkham, *Introduction to Superconductivity* (McGraw-Hill, New York, 1996).
[28] W. L. McMillan, Phys. Rev. **167**, 331 (1967).
[29] W. Yue-Qin, Y. Lan-Feng, and Y. Jin-Long, Chinese Phys. Lett. **25**, 3036 (2008).
[30] W. E. Pickett, Braz. J. Phys. **33**, 695 (2003).
[31] M. Kriener, Y. Maeno, T. Oguchi, Z.-A. Ren, J. Kato, T. Muranaka, and J. Akimitsu, Phys. Rev. B **78**, 024517 (2008).